insects

MDPI

Article

Tyramine-Centered Tyrosine Metabolism in Larval Heads Accompanies Light-Dependent Climbing in LdMNPV-Infected *Lymantria dispar*

Xiang Liu, Shuo Mei and Dun Wang *

Key Laboratory of Integrated Pest Management on the Loess Plateau of Ministry of Agriculture and Rural Affairs, Northwest A&F University, Yangling 712100, China; liuxiang_edu@126.com (X.L.); meishuo202412@126.com (S.M.)
* Correspondence: dunwang@foxmail.com; Tel.: +86-29-8709-1511

Simple Summary

Baculoviruses alter the behavior of their caterpillar hosts, and infected larvae often climb to elevated positions before death, a phenomenon called tree-top disease. The molecular changes that come with it are less clear. We measured climbing in gypsy moth larvae infected with a baculovirus and compared the heads of infected and uninfected larvae at two stages of infection using gene expression and metabolite profiling. Infected larvae climbed higher than controls only when light was available. Their heads first showed a broad response to infection and later a specific change in tyrosine metabolism, from which several neurotransmitters are made. Tyramine rose as climbing peaked, so it is a candidate link between infection and behavior.

Abstract

Tree-top disease is a behavioral syndrome of baculovirus-infected caterpillars, and the host molecular responses behind it remain unclear. We infected *Lymantria dispar* larvae with *Lymantria dispar* multiple nucleopolyhedrovirus (LdMNPV) and combined climbing assays, head transcriptomics and targeted metabolomics. Climbing height was measured in mock-inoculated larvae and at 3 and 6 days post-infection. Under white light, infected larvae climbed higher at both stages; in complete darkness, the three groups did not differ. RNA sequencing of whole heads found 1853, 2527 and 358 differentially expressed genes in the mock versus 3-day, mock vs. 6-day and 3-day vs. 6-day comparisons, respectively. Enrichment pointed to tyrosine metabolism, neuroactive ligand–receptor interaction and related amino-acid pathways. Targeted metabolomics found coordinated changes in biogenic amines and amino-acid metabolites, and tyramine rose most clearly, especially at 6 days. Integration connected tyrosine decarboxylase (*TDC*), tyrosine aminotransferase (*TAT1*) and dopamine N-acetyltransferases 1 and 2 (*DA-NAT1*, *DA-NAT2*) with the matching metabolites within tyrosine metabolism. Tree-top disease coincided with a staged molecular response in the larval head, and the data point to tyramine-centered tyrosine metabolism as a candidate link between LdMNPV infection and host behavior.

Keywords: *Lymantria dispar*; LdMNPV; tree-top disease; climbing behavior; head transcriptomics; neurotransmitter-targeted metabolomics; tyrosine metabolism; tyramine

Check for updates

Academic Editors: Maurizio Francesco Brivio and Maristella Mastore

Received: 5 November 2026
Revised: 19 November 2026
Accepted: 25 November 2026
Published: 27 November 2026

Copyright: © 2026 by the authors. Licensee MDPI, Basel, Switzerland. This article is an open access article distributed under the terms and conditions of the Creative Commons Attribution (CC BY) license.

1. Introduction

Lymantria dispar, the Asian gypsy moth, defoliates deciduous forests in its native and invaded ranges. Its outbreaks collapse when *Lymantria dispar* multiple nucleopolyhedrovirus (LdMNPV) replicates in the larvae and spreads among individuals. The virus is therefore commercialized as a biopesticide [1–3]. Larvae ingest occlusion bodies and die days later, after feeding stops and movement increases. The damage comes from these larvae, which feed on expanding foliage. Asian and North American types of LdMNPV differ in virulence and virulence genes, and the virus's genome and pathology have been described for both [4]. Tree-top disease is the syndrome whereby infected caterpillars move to higher, better-lighted areas before death. The ascent appears to be a response to light: infected *Spodoptera exigua* larvae exhibit positive phototaxis [5]. Since the extended-phenotype model [6], it has been debated whether the ecdysteroid UDP-glucosyltransferase gene (*egt*), which slows down death, is needed for the phenotype. Conversely, phototaxis is a mechanism employed by the host to defend against parasites [7] and immune challenge alone alters insect behavior [8]. The same climb fits both readings, parasite manipulation and host defense.

The silkworm *Bombyx mori* provides the most explicit time course. The climbing behavior occurs in stages and is resolved to the hour [9], and midgut-derived tachykinin links phototactic climbing to virus transmission [10]. Brain chemosensory protein 3 is necessary for enhanced locomotion [11] and adipokinetic hormone signaling has been shown to shift lipid distribution and to trigger climbing [12]. In *L. dispar*, transcriptomics has profiled the hyperactive stage [13], implicated phototransduction and circadian entrainment in light response [14] and linked PI3K/AKT with PTEN to the phenotype [15]. Most of these studies use whole larvae or a single time point, and none indicates which metabolic systems change when. The immune gene families that may underlie these responses are annotated in the gypsy moth genome [16].

Viral protein tyrosine phosphatase (*ptp*) does not appear to be necessary for baculoviruses to reach the central nervous system [17], and neither *ptp* nor *egt* is essential for enhanced locomotion in *Bombyx mandarina* [18]. A hormone metabolic disorder is sufficient to enhance locomotion in *B. mori* [19]. Amines coordinate metabolism and mobility: tyramine decreases the excitability of motoneurons while the tyramine/octopamine ratio tunes the locomotor output according to nutritional status [20]. Both amines come from tyrosine, which also feeds immune melanization. The two amines act in opposite directions on honeybee vision [21], octopamine receptor signaling in muscle and heart is needed for exercise adaptations [22], and dopamine D1 signaling controls turning through the central complex [23]. Neuromodulators of this class can turn visual avoidance into approach [24].

One pathway uses light onset to command deceleration in larvae [25]. In *Plutella xylostella*, biogenic amines regulate oviposition [26], tyramine acts through the type 1 tyramine receptor (TAR1) [27], and TAR1 knockout reduces oviposition and mating [28]. TAR1 is the best-studied amine receptor in this genus. Related amine receptors have been profiled in the same moth [29], and tyramine receptor variation is linked to a behavioral quantitative trait locus (QTL) in honeybees [30]. Arylalkylamine N-acetyltransferase 1 (AANAT1) inactivates dopamine and serotonin in astrocytes [31] and regulates midgut detoxification through reactive oxygen species (ROS)/CncC signaling [32]. The same enzyme acts in both amine clearance and xenobiotic handling.

Gut-derived octopamine promotes larval locomotion [33], and immune melanization is itself under selection as a defense [34]. Behavioral manipulation has been dissected in other parasite systems [35], and a single amine can reorganize neurobehavior [36]. Microbes, immune effectors and single amines can all change host movement, and which route dominates will differ between systems. Metabolomics of baculovirus infection has looked at silkworm hemolymph and midgut, where amino-acid pools shift [37,38], gut

metabolites track the microbiota [39], and midgut profiles differ with host resistance [40]. These tissues are systemic, sampled once, and not neural. We measured climbing height at 3 and 6 days post-inoculation (dpi) in light and darkness, profiled head transcripts at the same stages, and quantified 40 targeted metabolites. The three datasets were integrated to ask whether tree-top disease coincides with a stage-specific change in tyrosine metabolism.

2. Materials and Methods

2.1. Insect Rearing and LdMNPV Inoculation

About 500 *Lymantria dispar* larvae were collected in Changchun, Jilin Province, China (125.26° E, 43.95° N) on 17 October 2023. Hatchlings were reared singly in ventilated 25 mL plastic cups with roughly 2 cm^3 of artificial diet. Cups were held at 25 ± 1 °C and 60 ± 5% relative humidity on a 14:10 h (L:D) cycle, lights on 09:00 to 23:00. Diet was replaced every 48 h. Larvae that had molted twice after hatching counted as third instars.

Wild-type LdMNPV and the artificial diet came from the laboratory of Prof. Liang-Jian Qu (Chinese Academy of Forestry, Beijing, China); occlusion bodies (OBs) were purified as in Zhao et al. [41]. Newly ecdysed third instars were starved for 24 h and then inoculated by droplet feeding. The OB stock (2×10^9 OBs/mL) was mixed with an equal volume of 20% sucrose, giving a suspension of 1×10^9 OBs/mL in 10% sucrose, and each larva was offered 2 µL [41]. Controls received 2 µL of 10% sucrose. Only larvae that consumed the entire droplet; these were moved to individual cups with diet at 12 h post-inoculation (hpi) and held in an environmental chamber afterward.

2.2. Climbing Assay

Climbing was scored in mock-inoculated and LdMNPV-inoculated larvae at 3 and 6 dpi, in white light and in complete darkness. Each larva was placed individually in a clear cylinder (6 cm inner diameter, 50 cm in height) lined on the inside with mesh. Both ends were sealed with clear film pierced with six small ventilation holes, and a cube of artificial diet (approximately 3 cm^3) was placed at the bottom. The sides and base were wrapped in aluminum foil, and the cylinders were placed inside a black box that excluded room light, so light reached the larvae only from above through the clear film.

A broad-spectrum lamp positioned 30 cm above the cylinders provided the white-light treatment at an intensity of 2000 lux at the level of the larvae, following the same 14:10 h light:dark cycle used for rearing (lights on from 09:00 to 23:00), the same cycle used for rearing. The dark treatment was performed in constant darkness (DD) and lasted 2 h. Mock-inoculated larvae were held under the same light regime as infected larvae. Assays started between 11:00 and 13:00 and ran for 2 h; the height each larva had reached was recorded at the end. Each group had nine independent biological replicates of 15 larvae, and the mean height of those 15 larvae was the value analyzed.

2.3. Head Sample Collection and RNA Sequencing

Whole larval heads were collected for transcriptome and metabolome profiling. Mock-inoculated larvae were sampled at 3 dpi, and infected larvae at 3 or 6 dpi. Each biological replicate consisted of the pooled heads of five larvae, and three independent replicates were used per group. RNA was extracted with TRIzol reagent (Life Technologies, Carlsbad, CA, USA). Concentration and purity were measured on a NanoDrop 2000 spectrophotometer (Thermo Fisher Scientific, Wilmington, DE, USA); integrity was checked with the RNA Nano 6000 Assay Kit on an Agilent Bioanalyzer 2100 system (Agilent Technologies, Santa Clara, CA, USA).

Each library was prepared from 1 µg of total RNA using the Hieff NGS Ultima Dual-mode mRNA Library Prep Kit for Illumina (Yeasen Biotechnology, Shanghai, China),

following the manufacturer's protocol. Poly(A) RNA was enriched using poly-T magnetic beads and reverse transcribed to generate double-stranded complementary DNA (cDNA). Adapters were then ligated, and the products were amplified by polymerase chain reaction (PCR), and the libraries sequenced on an Illumina NovaSeq platform in 150 bp paired-end mode. Reads carrying adapters, poly-N tracts or low-quality bases were removed with the BMKCloud pipeline (Biomarker Technologies, Beijing, China). Clean reads were aligned to the *L. dispar* reference assembly (*Lymantria_dispar*.GCA_016802235.1.genome.fa) with HISAT2 [42], and transcripts were assembled with StringTie v2.2.1 [43]. Expression was normalized to FPKM (fragments per kilobase of transcript per million mapped fragments).

Three pairwise contrasts were tested: mock vs. LdMNPV_3d, mock vs. LdMNPV_6d, and LdMNPV_3d vs. LdMNPV_6d. Differential expression was analyzed in DESeq2 v1.30.1 [44] with a Wald test and a parametric dispersion fit. A gene was considered differentially expressed when its fold change was ≥2 or ≤0.5 and its Benjamini–Hochberg false discovery rate (FDR) was below 0.01. Gene Ontology (GO) and Kyoto Encyclopedia of Genes and Genomes (KEGG) enrichment analyses were performed using clusterProfiler v4.4.4 [45]. Gene set enrichment analysis (GSEA) was performed with 1000 permutations, and adjusted q values below 0.05 were taken as significant [46].

2.4. Targeted Neurotransmitter Metabolomics

Each metabolomics sample was a pool of five heads (approximately 20 mg of tissue). Of the 42 compounds in the panel, 40 passed preprocessing and were retained for analysis. A steel bead was added to each sample, and metabolites were extracted in 80 µL of ice-cold 0.1% formic acid in acetonitrile plus 20 µL of water. Vortexing lasted 60 s. The samples were then subjected to three homogenization rounds (240 s, 45 Hz), each with 5 min of sonication in an ice-water bath. Extracts were left overnight at −20 °C and centrifuged at 12,000 rpm for 15 min at 4 °C. An 80 µL aliquot of the supernatant was derivatized for 30 min at room temperature with 40 µL of 100 mM sodium carbonate and 40 µL of 2% benzoyl chloride [47]. Internal standard (10 µL of H-Std-a-Bz-DF) was added to 160 µL of the derivatized extract, and 40 µL of that mixture was diluted with 20 µL of water for injection.

Analytes were separated by ultra-high-performance liquid chromatography (UHPLC) on a Waters ACQUITY Premier system with an ACQUITY UPLC HSS T3 column (100 × 2.1 mm, 1.8 µm) at 40 °C. Mobile phase A was 0.1% formic acid with 1 mM ammonium acetate in water; mobile phase B was acetonitrile. The autosampler was kept at 10 °C, and the injection volume was 1 µL. Detection was performed on a SCIEX QTRAP 6500+ mass spectrometer (QTRAP 6500+ mass spectrometer, SCIEX, Framingham, MA, USA) in multiple-reaction monitoring mode [47], with an electrospray voltage of 5000 V, curtain gas at 35 psi, a source temperature of 400 °C and source gases 1 and 2 at 60 psi. Metabolites were identified and quantified in Skyline [48], and concentrations are given as nmol/g tissue.

Principal component analysis (PCA) was performed in SIMCA v16.0.2 using $\log_2$-transformed, mean-centered abundances. Compounds missing from more than half the samples of a group were dropped, and remaining missing values were imputed as half the lowest detected value. Pairwise group differences were tested with t tests. p values were Benjamini–Hochberg adjusted, and $q < 0.05$ was significant.

2.5. Integration of Transcriptome and Metabolome Data

For integration, expression values were transformed to $\log_2(\text{FPKM} + 1)$ and metabolite concentrations to $\log_2(\text{nmol/g})$. Spearman rank correlations between candidate genes and metabolites were computed across the mock, LdMNPV_3d and LdMNPV_6d samples.

Partial Spearman correlations with treatment group (mock, 3 dpi or 6 dpi) as covariate gave associations adjusted for group.

2.6. Statistical Analysis

Climbing heights were compared between groups with unpaired Student's *t* tests, with the mean of 15 larvae as the unit of analysis ($n = 9$ per group); the same test was applied to the light and dark treatments, and $p < 0.05$ was considered significant. Data are presented as mean ± s.e.m. Transcript, metabolite and correlation analyses followed Sections 2.3–2.5: DESeq2 with a Wald test (fold change ≥2 or ≤0.5; Benjamini–Hochberg FDR < 0.01) for differential expression, *t* tests with Benjamini–Hochberg correction across the 40 retained compounds ($q < 0.05$) for metabolites, and Spearman rank correlation with partial correlation adjusting for infection group ($n = 9$ samples) for gene–metabolite associations. Tests and figures were produced in GraphPad Prism v11.0.0.84; differential expression and enrichment used DESeq2 v1.30.1 and clusterProfiler v4.4.4. The data presented in this study are available in the Supplementary Materials (Minimal dataset, Tables S1–S7).

3. Results

3.1. LdMNPV Infection Increased Climbing Height Under Light

Climbing height was measured in a light-controlled chamber (Figure 1A), using nine biological replicates per group (15 larvae per replicate); values are means ± standard error of the mean (s.e.m.). In complete darkness, climbing height did not differ significantly among the three groups (mock: 22.6 ± 4.4 cm; LdMNPV_3d: 24.5 ± 4.1 cm and LdMNPV_6d: 18.7 ± 4.1 cm; Figure 1B). Heights in darkness also varied more widely among replicates, with s.e.m. values of 4.1 to 4.4 cm rather than 0.8 to 1.7 cm under light. Under light, mock larvae stayed low (8.9 ± 0.8 cm) whereas LdMNPV_3d (35.9 ± 1.6 cm, df = 16, $t = -15.476$, $p < 0.001$) and LdMNPV_6d (41.7 ± 1.7 cm, df = 16, $t = -18.057$, $p < 0.001$) climbed far higher (Figure 1C). LdMNPV_6d larvae also exceeded LdMNPV_3d larvae in climbing height by 5.8 cm (df = 16, $t = 2.5536$, $p = 0.021$; Figure 1C).

3.2. The Head Transcriptional Response Differed with Infection Stage

Head RNA sequencing identified 1853 differentially expressed genes (DEGs) in the mock vs. LdMNPV_3d comparison (625 upregulated, 1228 downregulated), 2527 in mock vs. LdMNPV_6d (912 upregulated, 1615 downregulated) and 358 in LdMNPV_3d vs. LdMNPV_6d (75 upregulated, 283 downregulated; Figure 2A). The three contrasts shared 81 DEGs (Figure 2B). A further 1022 DEGs were unique to mock vs. LdMNPV_6d, 484 to mock vs. LdMNPV_3d and 67 to LdMNPV_3d vs. LdMNPV_6d. Pairwise sharing was 1251 DEGs between mock vs. LdMNPV_3d and mock vs. LdMNPV_6d, 173 between mock vs. LdMNPV_6d and LdMNPV_3d vs. LdMNPV_6d, and 37 between mock vs. LdMNPV_3d and LdMNPV_3d vs. LdMNPV_6d (Figure 2B). The transcriptional response was largest at 6 dpi (2527 DEGs), and downregulated genes outnumbered upregulated genes in all three contrasts.

3.3. Enrichment Shifted from Xenobiotic and Carbohydrate Metabolism to Tyrosine Metabolism

The mock vs. LdMNPV_3d contrast produced a broad spread of up- and downregulated transcripts in the volcano plot (Figure 3A). GO annotation assigned these DEGs mainly to cellular and metabolic processes, intracellular and cellular anatomical components, and catalytic, binding and transporter functions (Figure 3B). KEGG enrichment identified metabolism of xenobiotics by cytochrome P450 ($q = 6.04 \times 10^{-12}$), pentose and glucuronate interconversions ($q = 3.12 \times 10^{-11}$) and insect hormone biosynthesis ($q = 3.62 \times 10^{-11}$) (Figure 3C).

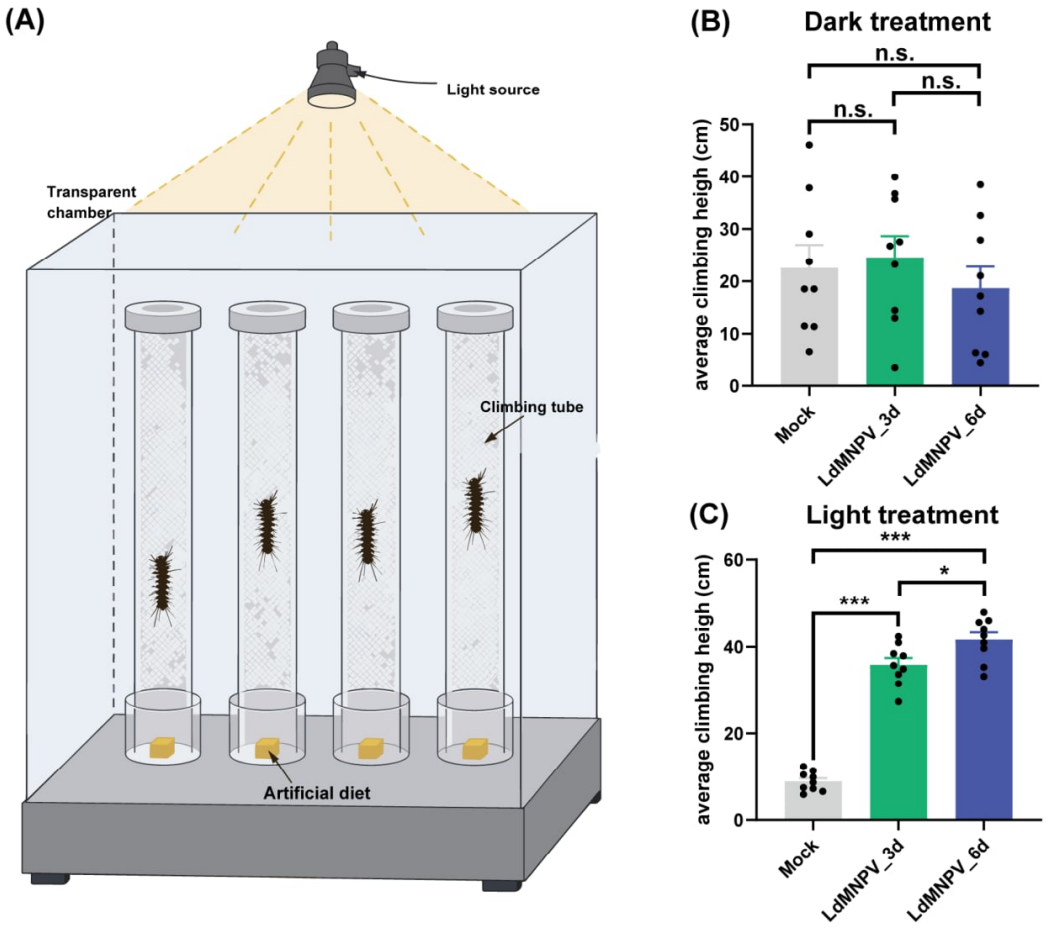


Figure 1. LdMNPV infection increased climbing height under light. (**A**) Schematic of the climbing assay, showing the transparent chamber, climbing tubes, artificial diet and overhead light source. (**B**,**C**) Mean climbing height of mock-inoculated, LdMNPV_3d and LdMNPV_6d larvae under dark (**B**) and light (**C**) conditions. Each point represents one biological replicate (15 larvae per replicate; $n = 9$ per group); bars show means and error bars show s.e.m. Statistical comparisons used unpaired Student's *t*-tests; significance annotations are shown above the brackets. * $p < 0.05$; *** $p < 0.001$; n.s., not significant ($p \geq 0.05$).

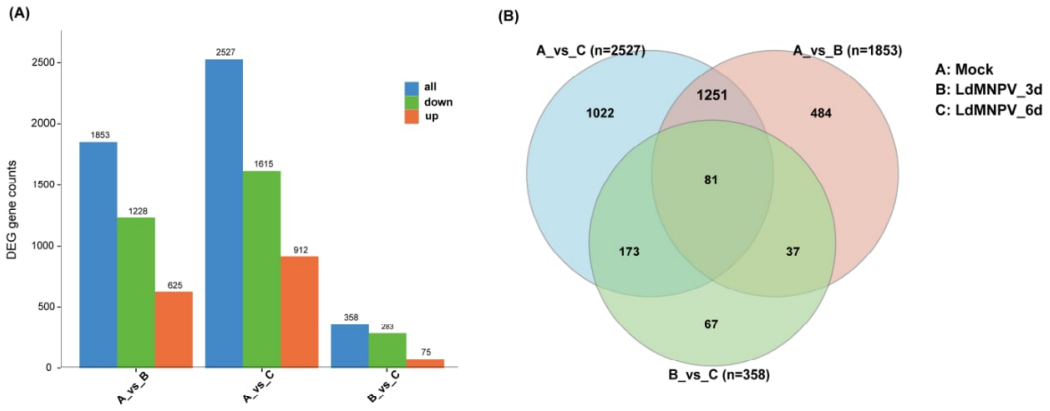


Figure 2. Differentially expressed genes across LdMNPV infection stages. (**A**) Counts of all, downregulated and upregulated genes in the mock vs. LdMNPV_3d, mock vs. LdMNPV_6d and LdMNPV_3d vs. LdMNPV_6d contrasts. (**B**) Venn diagram showing the overlap of DEG sets among the three contrasts. A, mock; B, LdMNPV_3d; C, LdMNPV_6d. DEGs were defined using an absolute fold-change threshold of 2 and a Benjamini–Hochberg FDR below 0.01.

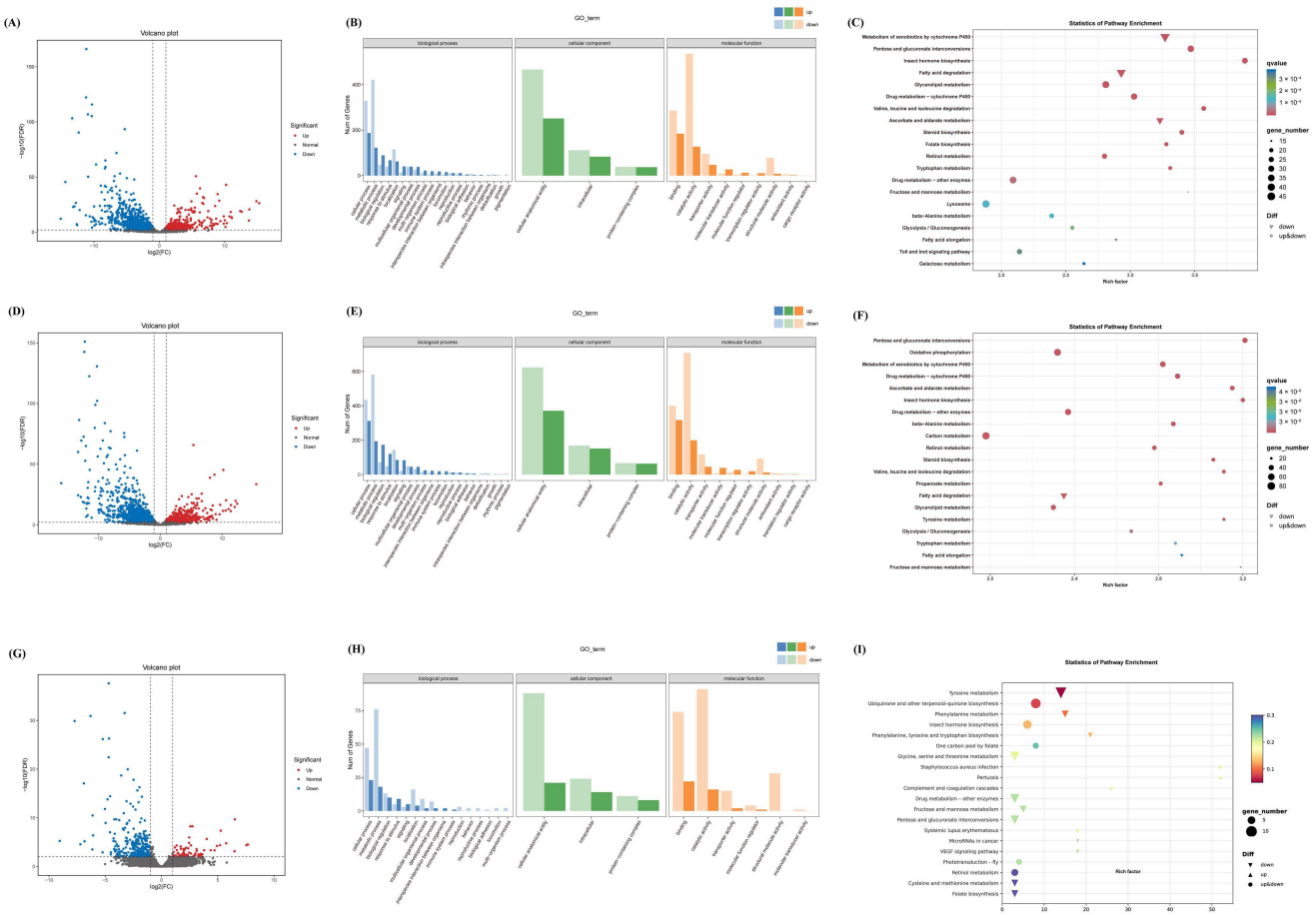


Figure 3. Stage-specific transcriptional enrichment during LdMNPV infection. For the mock vs. LdMNPV_3d contrast (**A**–**C**), mock vs. LdMNPV_6d contrast (**D**–**F**) and LdMNPV_3d vs. LdMNPV_6d contrast (**G**–**I**), panels show volcano plots (**A**,**D**,**G**), Gene Ontology enrichment (**B**,**E**,**H**) and KEGG pathway enrichment (**C**,**F**,**I**), respectively. Volcano-plot colors denote upregulated, non-significant and downregulated transcripts. In the enrichment dot plots, point size indicates gene number and color indicates the adjusted enrichment value; symbols distinguish the direction of the enriched gene set as shown in the plot.

The mock vs. LdMNPV_6d contrast had the largest DEG set and a wider range of fold changes (Figure 3D). Its GO profile retained the cellular, metabolic and catalytic terms seen at 3 dpi, with more genes assigned to intracellular organization and to binding and catalytic functions (Figure 3E). The most strongly enriched KEGG pathways were pentose and glucuronate interconversions ($q = 1.78 \times 10^{-13}$), metabolism of xenobiotics by cytochrome P450 and oxidative phosphorylation (both $q = 2.87 \times 10^{-12}$), insect hormone biosynthesis ($q = 1.11 \times 10^{-10}$) and β-alanine metabolism ($q = 3.22 \times 10^{-10}$) (Figure 3F).

The LdMNPV_3d vs. LdMNPV_6d contrast contained fewer DEGs and was dominated by downregulated transcripts (Figure 3G). GO annotation again emphasized cellular processes, intracellular components and catalytic or binding functions (Figure 3H). Tyrosine metabolism was the leading enriched KEGG pathway (14 downregulated genes, $q = 3.08 \times 10^{-11}$); phenylalanine metabolism ($q = 2.07 \times 10^{-3}$), ubiquinone and other terpenoid-quinone biosynthesis ($q = 5.60 \times 10^{-4}$) and insect hormone biosynthesis ($q = 0.0407$) were also enriched (Figure 3I).

3.4. Tyramine Was the Only Metabolite with an FDR-Significant Change

Targeted profiles separated the three groups in principal-component space, with PC1 and PC2 explaining 46.4% and 15.3% of the variances (Figure 4A), respectively. Tyramine

was the only compound above the differential threshold in the LdMNPV_6d vs. mock comparison ($\log_2$ fold change 5.2; Figure 4B). After correction, no compound differed in the LdMNPV_3d vs. mock or LdMNPV_6d vs. LdMNPV_3d comparisons (Figure 4C). The heatmap showed stage-dependent shifts across the panel, with LdMNPV_6d samples separating from mock and LdMNPV_3d (Figure 4D).

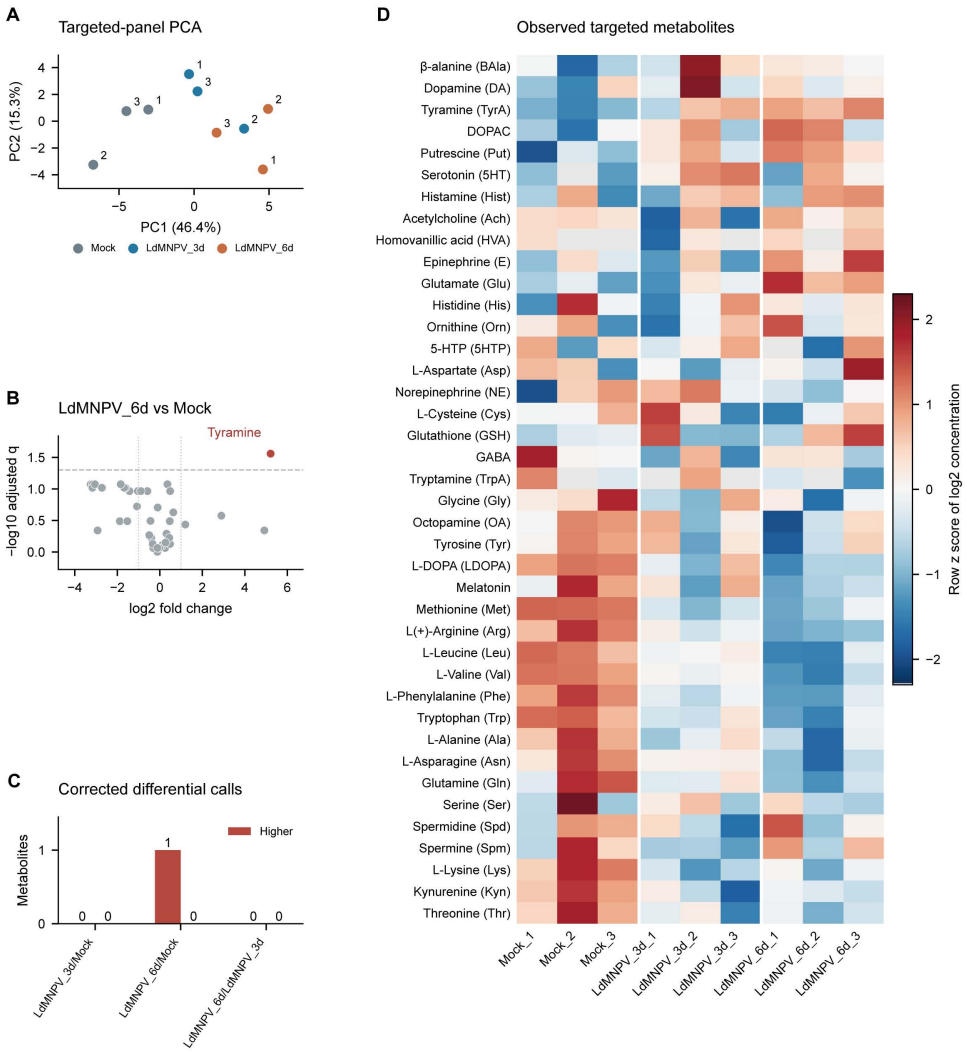


Figure 4. Global structure of the targeted metabolomics response. (**A**) Principal-component analysis of the targeted metabolite panel; numbers indicate biological replicates. (**B**) Differential metabolite plot for LdMNPV_6d vs. mock, with tyramine highlighted. (**C**) Number of metabolites passing the corrected differential threshold in each pairwise comparison. (**D**) Heatmap of row-standardized $\log_2$ metabolite concentrations across the three groups. In panel B, the red dot represents tyramine, the only significantly increased metabolite after Benjamini–Hochberg correction ($q < 0.05$); gray dots represent metabolites without statistically significant changes ($q \geq 0.05$).

Tyramine increased from mock to LdMNPV_3d and reached significance at 6 dpi ($q = 0.232$ and 0.028 for the 3-day and 6-day comparisons with mock; Figure 5A). Octopamine ($q = 0.500$ and 0.325) and dopamine ($q = 0.500$ and 0.512) were unchanged after FDR correction, and serotonin varied across stages without passing the threshold ($q = 0.114$ and 0.367; Figure 5B–D). Histamine ($q = 0.746$ and 0.596), acetylcholine ($q = 0.444$ and 0.778) and γ-aminobutyric acid (GABA; $q = 0.444$ and 0.540) showed no pairwise differences (Figure 5E–G). Glutamate ($q = 0.746$ and 0.084) and L-3,4-dihydroxyphenylalanine

(L-DOPA; $q = 0.326$ and 0.084) came closest to the threshold, both at 6 dpi (Figure 5H,I). No other measured metabolite increased significantly in any comparison.

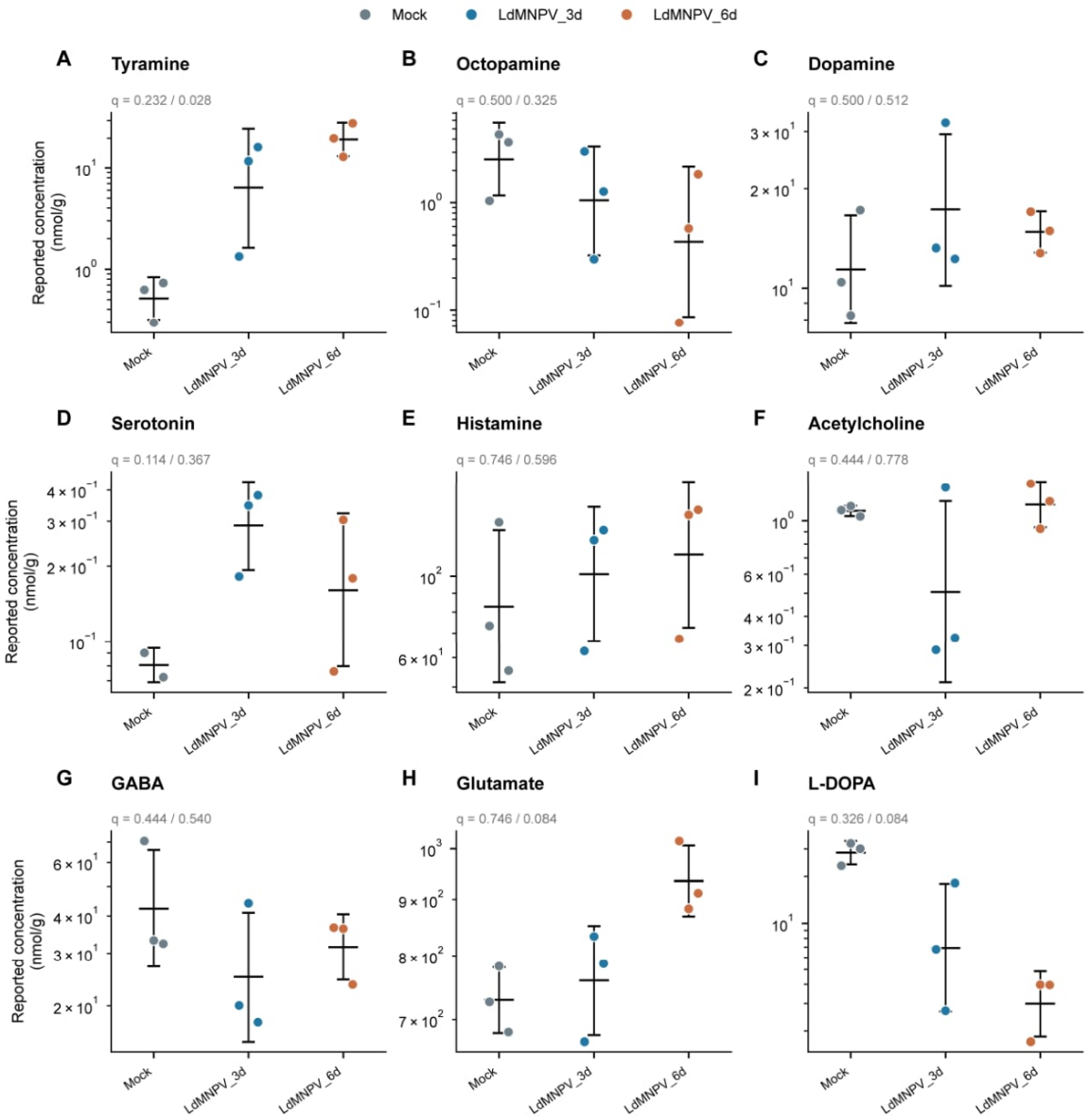


Figure 5. Targeted measurements of neurotransmitters and related metabolites. Concentrations of tyramine (**A**), octopamine (**B**), dopamine (**C**), serotonin (**D**), histamine (**E**), acetylcholine (**F**), GABA (**G**), glutamate (**H**) and L-DOPA (**I**) in mock-inoculated, LdMNPV_3d and LdMNPV_6d larval heads. Points show individual biological replicates, and the plotted bars and error bars summarize each group. The *q* values printed in each panel are the FDR-adjusted comparisons with mock for the 3-day and 6-day groups, respectively.

3.5. Integrated Analysis Associated Tyrosine Pathway Genes with Their Metabolites

Integration of the transcriptome and metabolome data identified tyrosine metabolism and neuroactive ligand–receptor interaction among the pathways repeatedly enriched in the RNA data. Tryptophan metabolism, *β*-alanine metabolism and valine, leucine and isoleucine degradation were also enriched (Figure 6A). Metabolite mapping supported these assignments in all three pairwise comparisons, although the number of mapped metabolites varied by pathway and contrast (Figure 6B). Pooled and group-adjusted correlations differed in sign or size among pathways (Figure 6C).

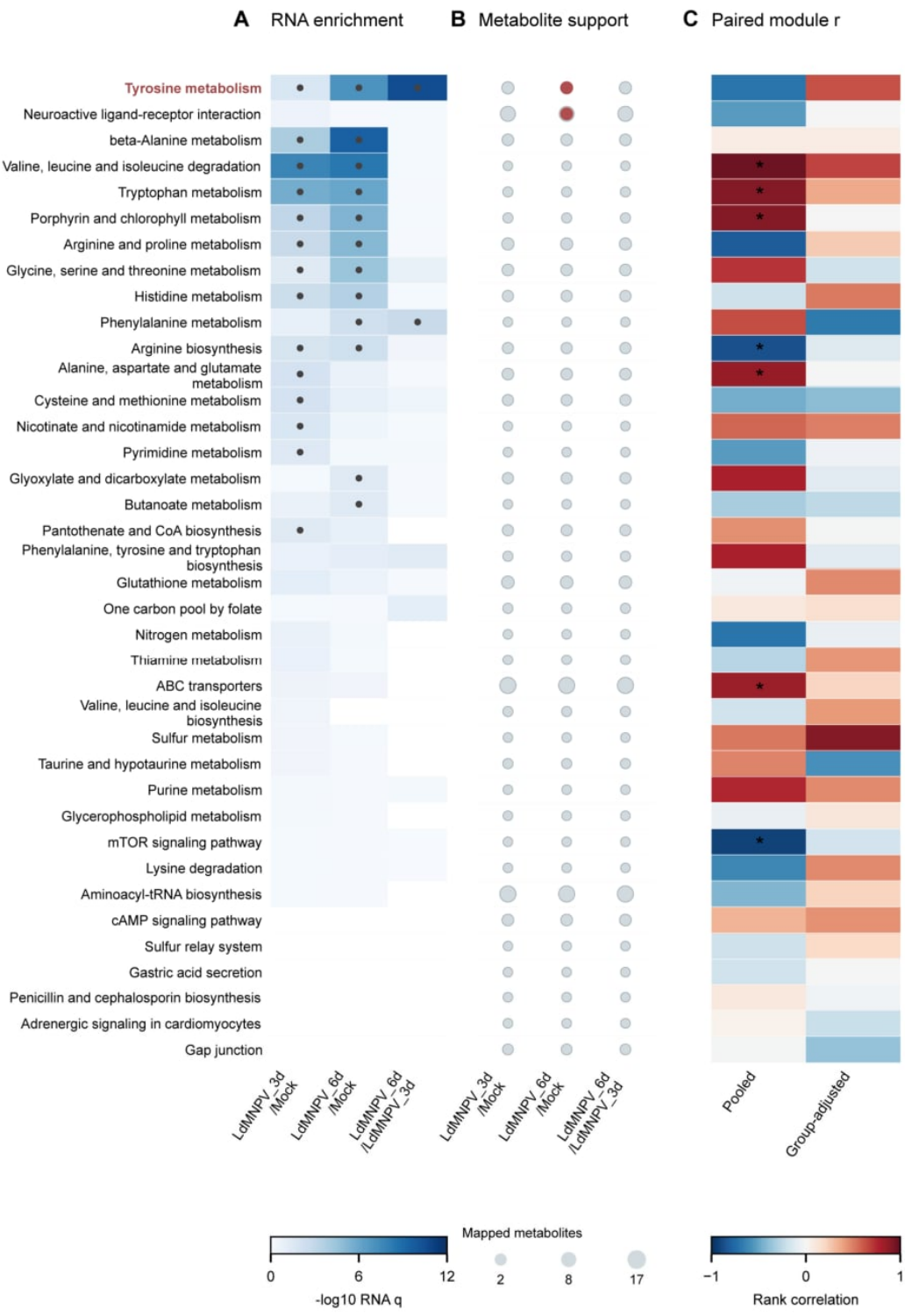


Figure 6. Joint pathway-level analysis of transcript and metabolite data. (**A**) RNA-seq pathway enrichment across the three pairwise contrasts. (**B**) Metabolites mapped to the corresponding pathways in each contrast; circle size indicates the number of mapped metabolites. (**C**) Spearman rank correlations for paired pathway modules calculated either from pooled samples or after adjustment for infection group. Color scales and significance symbols follow the definitions shown in the panels. In panel A, black dots indicate significantly enriched pathways (Benjamini–Hochberg-adjusted $q < 0.05$) in the corresponding comparisons; blue shading represents $-\log_{10}(q)$. In panel C, * indicates a statistically significant correlation ($p < 0.05$).

The integrated heatmaps showed coordinated stage-dependent changes between annotated transcripts and matched metabolites. Tyrosine aminotransferase (*TAT1*) and the dopamine N-acetyltransferases *DA-NAT1* and *DA-NAT2* were expressed at lower levels in the infected comparisons. The matched metabolites covered the tyrosine branch (tyrosine, tyramine, L-DOPA and dopamine), 3,4-dihydroxyphenylacetic acid (DOPAC), the tryptophan branch (tryptophan and kynurenine) and the GABA branch (glutamate and GABA) (Figure 7A,B). Tyrosine decarboxylase (*TDC*) and tyramine correlated positively across the nine samples ($r = +0.60$, $p = 0.088$), and the correlation weakened after group adjustment ($r = +0.28$, $p = 0.54$; Figure 7C). *TAT1* and tyramine correlated negatively in the pooled analysis ($r = -0.38$, $p = 0.31$) and positively after adjustment ($r = +0.77$, $p = 0.043$; Figure 7D). Tryptophan 2,3-dioxygenase (*TDO*) and tryptophan showed weak correlations in both analyses ($r = +0.18$, $p = 0.64$ and $r = +0.20$, $p = 0.67$, respectively; Figure 7E).

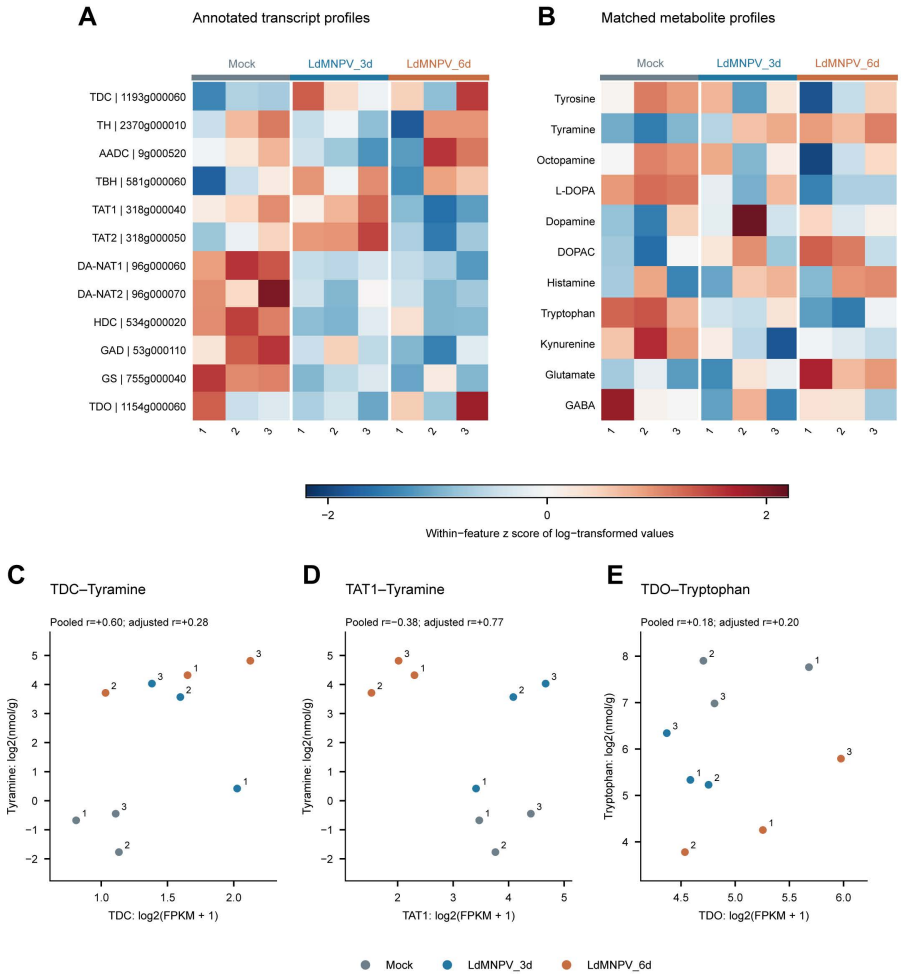


Figure 7. Coordinated transcript and metabolite profiles for candidate pathways. (**A**) Standardized expression profiles for annotated transcripts, including *TDC*, *TAT1*, *DA-NAT1* and *DA-NAT2*. (**B**) Matched profiles for tyrosine-branch, tryptophan-branch and GABA-branch metabolites. (**C**–**E**) Associations between *TDC* and tyramine, *TAT1* and tyramine, and *TDO* and tryptophan, respectively. Points are biological replicates; colors denote mock, LdMNPV_3d and LdMNPV_6d samples. Pooled and group-adjusted correlation coefficients are reported above each scatter plot.

The summary fold-change matrix captured the same selective response. Aromatic L-amino acid decarboxylase (*AADC*) fell in mock vs. LdMNPV_3d, *TAT1* fell in both comparisons involving LdMNPV_6d, and *DA-NAT1* and *DA-NAT2* fell in the mock vs. infected comparisons (Figure 8A). Among the matched metabolites, tyramine rose by $\log_2$

fold changes of +4.2, +5.2 and +1.1 in the LdMNPV_3d vs. mock, LdMNPV_6d vs. mock and LdMNPV_6d vs. LdMNPV_3d comparisons, respectively. Only the 6-day vs. mock comparison was significant. L-DOPA fell by −1.6, −3.2 and −1.5, and DOPAC rose by +1.9, +2.9 and +1.0, in the same order (Figure 8B).

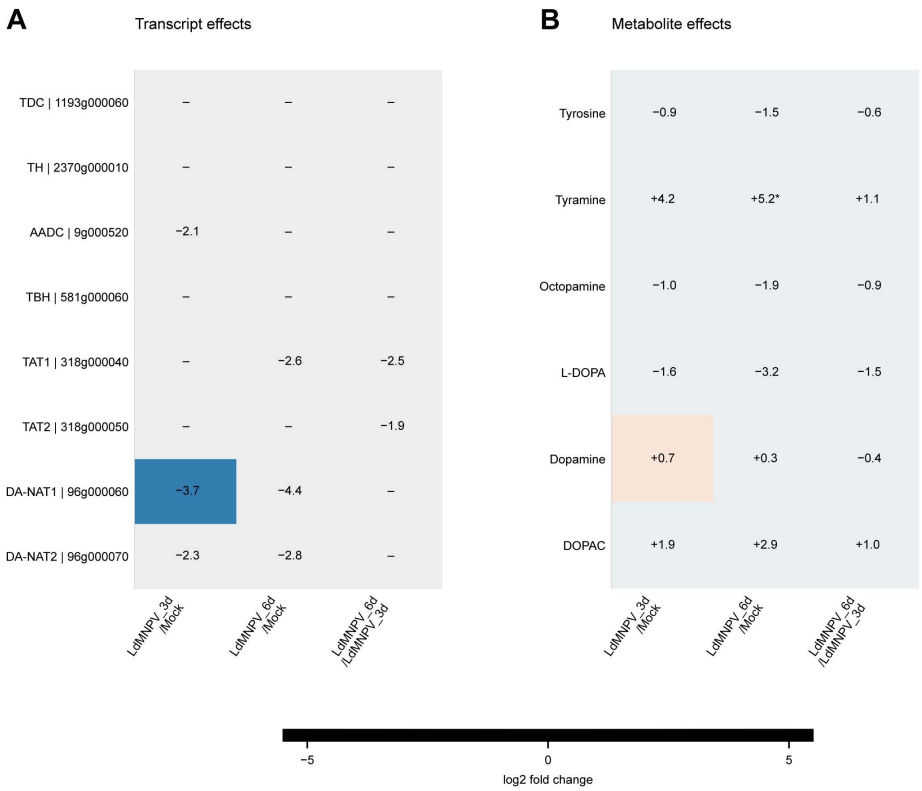


Figure 8. Fold-change matrix for tyrosine-pathway transcripts and matched metabolites. (**A**) Transcript $\log_2$ fold changes for the three pairwise contrasts. (**B**) Corresponding metabolite $\log_2$ fold changes for tyrosine, tyramine, octopamine, L-DOPA, dopamine and DOPAC. Cells marked with an asterisk indicate a statistically significant corrected comparison as shown in the matrix; dashes indicate that no differential call was made. In panel B, * indicates a statistically significant difference after Benjamini–Hochberg correction ($q < 0.05$).

4. Discussion

Under white light, infected larvae climbed four times higher than mock-inoculated larvae at 3 dpi and five times higher at 6 dpi. In darkness the three groups did not differ, so general hyperactivity does not explain the result. Heads from the same animals carried a stage-dependent transcriptional program. The 1853 genes that differed at 3 dpi and 2527 genes at 6 dpi were dominated by downregulated genes of the tyrosine metabolism pathway, of which 14 pathway genes passed the threshold. Among the amines, tyramine rose by 3 dpi (approximately 18-fold) and 6 dpi (approximately 37-fold) after correction (significant at 6 dpi only), while dopamine, octopamine, serotonin, histamine, acetylcholine and GABA remained flat. The transcript, pathway and metabolite readouts all indicate the same branch and step of the tyrosine metabolism. As they were part of a single experiment, any mismatch between them is not a batch or season effect. Oxidative phosphorylation at 6 dpi may be a way of balancing energy costs of continuous climbing and energy costs of viral replication; it does not necessarily refer to the nervous system. Climbing was already present at timepoint 1, so the trigger was prior to 3 dpi and the amine peak was consolidation, not onset. If tyramine is a causal factor, it would have to be activated before the appearance of the behavior (that is, before the first sampling); otherwise, it can only sustain it.

Three systems have described the tree-top disease, based on three different types of evidence; phototaxis in *S. exigua* [5], hourly staging in *B. mori* [9] and whole-larva transcription in *L. dispar* [13]. Whether the behavior is for the purpose of transmission has been a matter of debate since the extended-phenotype model [6]. The program here comprises two stages. The enrichment was focused on cytochrome P450, pentose and glucuronate interconversions and insect hormone biosynthesis at 3 dpi. This is characteristic of detoxification and an endocrine response. The enriched set continued to include oxidative phosphorylation and metabolism of β-alanine by 6 dpi, the latter of which is a precursor to the production of the cuticle, and the increase in levels of β-alanine coincided with decreases in *DA-NAT* transcripts, consistent with a larva being stalled before the developmental threshold. The 3–6 dpi contrast highlights the transition, and the signal for tyrosine is associated with the later stage.

Tyramine has built up without transcription induction of its synthesis. There was a positive correlation between *TDC* expression and tyramine concentration across nine samples ($r = 0.60$; $p = 0.088$) that was not significant and reduced to $r = 0.28$ after adjusting for infection group. *TAT1* and tyramine went the other way when pooled ($r = -0.38$) and the same way after adjustment ($r = 0.77$, $p = 0.043$). If the pooled coefficient is inverted after adjustment, it is due to a shift between groups, and the groups are different on both variables. The mechanistically relevant component is the within-group component, which cannot be estimated reliably because it rests on only 3 points per group. The firmer pathway level result is the 14 coordinately downregulated genes with the large accumulation of the downstream amine. The 3 dpi comparison alone would be misleading: there, tyramine was $\log_2$ fold change 4.2 (5.2 at 6 dpi), but q was 0.232, not 0.028, because estimates were based on three pooled replicates, which make the estimate imprecise. The enzyme step that results in accumulation is not known, and *TDC* transcription is not followed by accumulation. A separate question is what the additional tyramine might do. Tyramine reduces motoneuron output and the tyramine/octopamine ratio modulates the locomotor output [20]. The Lepidoptera tyramine receptor, TAR1, signals behavior [27]; knockout of TAR1 alters behavior in *P. xylostella* [28], and variation in the receptor corresponds to variation in behavior in honeybees [30]. The concentration of tyramine increased and the concentration of octopamine remained the same, creating a ratio that changed in one direction. The step at which the ratio changes is not known, as tyramine β-hydroxylase (*TβH*) was not measured. Less conversion, less reuptake and less oxidation are all options, and the flat octopamine pool rules out the possibility that more conversion caused the increase. If the ratio is the important factor and not the concentration, the behavior should remain unchanged relative to controls if both amines are increased proportionally.

Climbing was reliant on light, and thus the effect probably involved visual processing. These two amines have opposing effects on the vision of honeybees [21] and, in flying *Drosophila*, neuromodulators can switch visual avoidance to approach [24]. The handling of a light cue can change with a change of amine tone. If it is tyramine, which acts there, it would more likely modify the gain of the light to movement response and not the motor program. This assay cannot distinguish between greater height due to greater attraction and greater height due to more sustained walking or slower descent. The dopamine branch moved differently. L-DOPA, at 6 dpi, had decreased approximately 9-fold, DOPAC increased approximately 7-fold, and dopamine did not change, and *DA-NAT1* and *DA-NAT2* both decreased in the infected contrasts. The inactivation of dopamine and serotonin in astrocytes depends on AANAT1 [31], which is induced during midgut detoxification [32] and fits a detoxification capacity shift without calling on a neuron-specific change. The tyramine and dopamine branches could be coupled by a shared precursor pool, but steady state pools do not reveal this; their opposite directions point to two different pools, not driven by one.

There are two options, as opposed to the neural reading. Tyrosine is the substrate for phenoloxidase-based melanization [49], melanization capacity has been shown to affect susceptibility to baculovirus [50], and systemic immune activation would draw tyrosine into melanin. This would result in a decrease of the transcripts in the tyrosine-pathway without any neural change, and it is what is seen with the transcripts; however, it does not explain the rise in the tyramine, as melanization consumes the precursor. Antimicrobial peptides and Toll signaling play a role in host immunity against LdMNPV [51,52]. A reasonable pathway can be proposed for the diversion and a prediction made: if phenoloxidase activity increases as the tyrosine-pathway transcripts decrease, melanin levels should increase in hemolymph. The second option is "microbial." Bacteria in the gut produce tyramine which influences the sensory behavior of the host [53]; microbiota facilitates baculovirus infection [54]; and the gut bacteria community changes with baculovirus infection [41]. Therefore, a hemolymph-borne contribution to the head pool cannot be excluded. The presence of the amine would be indicative of systemic infection if of microbial origin, not a signal generated in the head.

Data is modeled by a staged model. Detoxification and endocrine response occur first, convergence on tyrosine follows—climbing peaks. Tyramine is the only amine that changed and is a candidate small molecule that acts on sensory and motor circuits in opposition to octopamine. A cadaver above the foliage also disperses occlusion bodies over a larger area [6], and ascent only took place when light was present.

Study Limitations

This is still a correlative study. The infection was manipulated and the amine chemistry was only measured, therefore tyramine cannot be conclusively proven to be the cause of the ascent. There are three pools, each with five heads, that are suitable for pathway-level calls but not for tissue assignment; and the correlations are based on 9 samples. In addition, 6 dpi infected larvae are compared with younger, mock-inoculated controls, because mock-inoculated heads were collected at 3 dpi only, so age is confounded with infection. External validity was limited to one viral dose, one host population and one photoperiod. Amine turnover and receptor expression were not measured. Additional experiments are needed to determine whether the amine shift is upstream of the climbing behavior.

To test necessity, *TDC* could be knocked down or TAR1 blocked prior to infection, followed by an assay in light and darkness; *TβH* knockdown would instead test the role of the ratio. Sampling at 1, 2, 3 and 6 dpi with brain-only tissue would place the amine relative to the onset of climbing. A germ-free comparison would separate the microbial contribution from the neural one and is feasible with the rearing protocol used here.

5. Conclusions

LdMNPV infection produced light-dependent ascent in *L. dispar*. Infected larvae climbed four to five times higher than mock-inoculated larvae under white light at 3 and 6 dpi, and in darkness no difference was detectable. Heads from the same animals went through a staged transcriptional reorganization that converged on downregulation of tyrosine metabolism between 3 and 6 dpi. Tyramine was the only biogenic amine that changed after correction, and it peaked at 6 dpi, when climbing height also peaked. Tyramine-centered tyrosine metabolism is therefore the candidate link between LdMNPV infection and host climbing behavior. The two-phase structure separates the endocrine and detoxification response common to any baculovirus infection from the tyrosine-specific change that comes with ascent. TAR1 and the tyramine/octopamine branch give a testable target for whether the amine shift causes the ascent.

Supplementary Materials: The following supporting information can be downloaded at: https://www.mdpi.com/article/10.3390/insects17121236/s1.

Author Contributions: Conceptualization, D.W.; methodology, X.L. and S.M.; software, X.L.; validation, X.L. and S.M.; formal analysis, X.L.; investigation, X.L. and S.M.; resources, D.W.; data curation, X.L.; writing—original draft preparation, X.L.; writing—review and editing, X.L. and D.W.; visualization, X.L.; supervision, D.W.; project administration, D.W.; funding acquisition, D.W. All authors have read and agreed to the published version of the manuscript.

Funding: This research was supported by a grant of the NSFC (32271894).

Institutional Review Board Statement: Not applicable. The study used *Lymantria dispar* larvae, an invertebrate species, and no ethical approval was required.

Informed Consent Statement: Not applicable.

Data Availability Statement: The data presented in this study are available in the Supplementary Material (Minimal dataset, Tables S1–S7), which reports the individual values underlying Figures 1–8. The raw RNA sequencing reads and the unprocessed metabolite data files are available from the corresponding author on reasonable request. They are not publicly deposited because they form part of a larger dataset from an ongoing project that includes unpublished experiments not reported in this article.

Acknowledgments: The authors thank Xiang-feng Jing in Northwest A&F University for his help on research instruments and manuscript editing.

Conflicts of Interest: The authors declare no conflicts of interest.

References

1. Keena, M.A.; Richards, J.Y. Comparison of Survival and Development of Gypsy Moth *Lymantria dispar* L. (Lepidoptera: Erebidae) Populations from Different Geographic Areas on North American Conifers. *Insects* **2020**, *11*, 260. [CrossRef]
2. Akhanaev, Y.; Pavlushin, S.; Yakimova, M.; Lebedeva, D.; Kurenshchikov, D.; Teshebaeva, Z.; Toshchakov, S.; Vyatkin, Y.; Kononchuk, A.; Ignatieva, A.; et al. Virulence and genome analysis of baculovirus isolates from different *Lymantria dispar* populations. *Sci. Rep.* **2025**, *15*, 28449. [CrossRef]
3. Liu, X.; Liu, T.X.; Wang, D. Sugar transporter protein gene LdST59 of *Lymantria dispar* mediates lethality of larvae infected by its viral pathogen, LdMNPV. *Pestic. Biochem. Physiol.* **2026**, *217*, 106871. [CrossRef]
4. Harrison, R.L.; Rowley, D.L.; Keena, M.A. Pathology and genome sequence of a *Lymantria dispar* multiple nucleopolyhedrovirus (LdMNPV) isolate from Heilongjiang, China. *J. Invertebr. Pathol.* **2020**, *177*, 107495. [CrossRef]
5. van Houte, S.; van Oers, M.M.; Han, Y.; Vlak, J.M.; Ros, V.I.D. Baculovirus infection triggers a positive phototactic response in caterpillars to induce 'tree-top' disease. *Biol. Lett.* **2014**, *10*, 20140680. [CrossRef]
6. Ros, V.I.D.; van Houte, S.; Hemerik, L.; van Oers, M.M. Baculovirus-induced tree-top disease: How extended is the role of egt as a gene for the extended phenotype? *Mol. Ecol.* **2015**, *24*, 249–258. [CrossRef]
7. Horn, C.J.; Wasylenko, J.A.; Luong, L.T. Scared of the dark? Phototaxis as behavioural immunity in a host–parasite system. *Biol. Lett.* **2022**, *18*, 20210531. [CrossRef]
8. Limberger, G.M.; Esteves, K.P.; Halal, L.M.; Nery, L.E.M.; da Fonseca, D.B. Chronic immune challenge is detrimental to female survival, feeding behavior, and reproduction in the field cricket *Gryllus assimilis* (Fabricius, 1775). *J. Comp. Physiol. B* **2022**, *192*, 423–434. [CrossRef]
9. Hikida, H.; Katsuma, S. High-resolution analysis of baculovirus-induced host manipulation in the domestic silkworm, *Bombyx mori*. *Parasitology* **2021**, *148*, 105–109. [CrossRef]
10. Zhu, L.; Liu, X.; Cai, L.; Li, Z.; Liu, C.; Liu, X. Baculoviruses hijack host midgut-derived tachykinin to regulate phototactic climbing behavior and promote viral transmission. *Proc. Natl. Acad. Sci. USA* **2026**, *123*, e2524226123. [CrossRef]
11. Feng, M.; Fei, S.; Papakyriakou, A.; Christodoulou, E.; Lai, W.; Luo, W.; Xia, J.; Huang, Y.; Zographos, S.E.; Swevers, L.; et al. Chemosensory protein 3 is a brain host factor for the induction of enhanced-locomotory activity in the BmNPV-silkworm infection model. *PLoS Pathog.* **2025**, *21*, e1013701. [CrossRef]
12. Zhu, L.; Xie, Y.; Liu, C.; Cheng, J.; Shen, Z.; Liu, X.; Cai, L.; Ning, X.; Zhang, S.; Li, Z.; et al. Baculoviruses manipulate host lipid metabolism via adipokinetic hormone signaling to induce climbing behavior. *PLoS Pathog.* **2025**, *21*, e1012932. [CrossRef]
13. Bhattarai, U.R.; Katuwal Bhattarai, M.; Li, F.; Wang, D. Insights into the Temporal Gene Expression Pattern in *Lymantria dispar* Larvae During the Baculovirus Induced Hyperactive Stage. *Virol. Sin.* **2018**, *33*, 345–358. [CrossRef]

14. Bhattarai, U.R.; Li, F.; Katuwal Bhattarai, M.; Masoudi, A.; Wang, D. Phototransduction and circadian entrainment are the key pathways in the signaling mechanism for the baculovirus induced tree-top disease in the lepidopteran larvae. *Sci. Rep.* **2018**, *8*, 17528. [CrossRef]
15. Li, F.; Liu, L.; Yu, X.; Rensing, C.; Wang, D. The PI3K/AKT Pathway and PTEN Gene Are Involved in "Tree-Top Disease" of *Lymantria dispar*. *Genes* **2022**, *13*, 247. [CrossRef]
16. Zhang, J.; Cong, Q.; Rex, E.A.; Hallwachs, W.; Janzen, D.H.; Grishin, N.V.; Gammon, D.B. Gypsy moth genome provides insights into flight capability and virus–host interactions. *Proc. Natl. Acad. Sci. USA* **2019**, *116*, 1669–1678. [CrossRef]
17. Gasque, S.N.; Han, Y.; van der Ham, I.; van Leeuwen, D.; van Oers, M.M.; Haverkamp, A.; Ros, V.I.D. Baculovirus entry into the central nervous system of *Spodoptera exigua* caterpillars is independent of the viral protein tyrosine phosphatase. *Open Biol.* **2024**, *14*, 230278. [CrossRef]
18. Kokusho, R.; Katsuma, S. *Bombyx mori* nucleopolyhedrovirus ptp and egt genes are dispensable for triggering enhanced locomotory activity and climbing behavior in *Bombyx mandarina* larvae. *J. Invertebr. Pathol.* **2021**, *183*, 107604. [CrossRef]
19. Li, Y.; Zhang, J.; Zhao, S.; Wu, X. BmNPV-induced hormone metabolic disorder in silkworm leads to enhanced locomotory behavior. *Dev. Comp. Immunol.* **2021**, *121*, 104036. [CrossRef]
20. Schützler, N.; Girwert, C.; Hügli, I.; Mohana, G.; Roignant, J.Y.; Ryglewski, S.; Duch, C. Tyramine action on motoneuron excitability and adaptable tyramine/octopamine ratios adjust *Drosophila* locomotion to nutritional state. *Proc. Natl. Acad. Sci. USA* **2019**, *116*, 3805–3810. [CrossRef]
21. Schilcher, F.; Thamm, M.; Strube-Bloss, M.; Scheiner, R. Opposing Actions of Octopamine and Tyramine on Honeybee Vision. *Biomolecules* **2021**, *11*, 1374. [CrossRef]
22. Sujkowski, A.; Gretzinger, A.; Soave, N.; Todi, S.V.; Wessells, R. Alpha- and beta-adrenergic octopamine receptors in muscle and heart are required for *Drosophila* exercise adaptations. *PLoS Genet.* **2020**, *16*, e1008778. [CrossRef]
23. Kottler, B.; Faville, R.; Bridi, J.C.; Hirth, F. Inverse Control of Turning Behavior by Dopamine D1 Receptor Signaling in Columnar and Ring Neurons of the Central Complex in *Drosophila*. *Curr. Biol.* **2019**, *29*, 567–577.e6. [CrossRef]
24. Cheng, K.Y.; Colbath, R.A.; Frye, M.A. Olfactory and Neuromodulatory Signals Reverse Visual Object Avoidance to Approach in *Drosophila*. *Curr. Biol.* **2019**, *29*, 2058–2065.e2. [CrossRef]
25. Gong, C.; Ouyang, Z.; Zhao, W.; Wang, J.; Li, K.; Zhou, P.; Zhao, T.; Zheng, N.; Gong, Z. A Neuronal Pathway that Commands Deceleration in *Drosophila* Larval Light-Avoidance. *Neurosci. Bull.* **2019**, *35*, 959–968. [CrossRef]
26. Li, F.; Li, K.; Wu, L.J.; Fan, Y.L.; Liu, T.X. Role of Biogenic Amines in Oviposition by the Diamondback Moth, *Plutella xylostella* L. *Front. Physiol.* **2020**, *11*, 475. [CrossRef]
27. Ma, H.; Huang, Q.; Lai, X.; Liu, J.; Zhu, H.; Zhou, Y.; Deng, X.; Zhou, X. Pharmacological Properties of the Type 1 Tyramine Receptor in the Diamondback Moth, *Plutella xylostella*. *Int. J. Mol. Sci.* **2019**, *20*, 2953. [CrossRef]
28. Zheng, W.; Ma, H.; Liu, Z.; Zhou, Y.; Zhu, H.; Liu, J.; Zhang, C.; Liu, Z.; Zhou, X. Knockout of tyramine receptor 1 results in a decrease of oviposition, mating, and sex pheromone biosynthesis in female *Plutella xylostella*. *Pest Manag. Sci.* **2023**, *79*, 3903–3912. [CrossRef]
29. Liu, T.; Zhan, X.; Yu, Y.; Wang, S.; Lu, C.; Lin, G.; Zhu, X.; He, W.; You, M.; You, S. Molecular and pharmacological characterization of biogenic amine receptors from the diamondback moth, *Plutella xylostella*. *Pest Manag. Sci.* **2021**, *77*, 4462–4475. [CrossRef]
30. Wang, Y.; Amdam, G.V.; Daniels, B.C.; Page, R.E., Jr. Tyramine and its receptor TYR1 linked behavior QTL to reproductive physiology in honey bee workers (*Apis mellifera*). *J. Insect Physiol.* **2020**, *126*, 104093. [CrossRef]
31. Davla, S.; Artiushin, G.; Li, Y.; Chitsaz, D.; Li, S.; Sehgal, A.; van Meyel, D.J. AANAT1 functions in astrocytes to regulate sleep homeostasis. *eLife* **2020**, *9*, e53994. [CrossRef]
32. Zeng, T.; Teng, F.Y.; Wei, H.; Lu, Y.Y.; Xu, Y.J.; Qi, Y.X. AANAT1 regulates insect midgut detoxification through the ROS/CncC pathway. *Commun. Biol.* **2024**, *7*, 808. [CrossRef]
33. Hu, J.; Bi, R.; Luo, Y.; Wu, K.; Jin, S.; Liu, Z.; Jia, Y.; Mao, C.X. The gut microbiome promotes locomotion of *Drosophila* larvae via octopamine signaling. *Insect Sci.* **2025**, *32*, 277–289. [CrossRef]
34. Smith, D.F.Q.; Camacho, E.; Thakur, R.; Barron, A.J.; Dong, Y.; Dimopoulos, G.; Broderick, N.A.; Casadevall, A. Glyphosate inhibits melanization and increases susceptibility to infection in insects. *PLoS Biol.* **2021**, *19*, e3001182. [CrossRef]
35. Elya, C.; Lavrentovich, D.; Lee, E.; Pasadyn, C.; Duval, J.; Basak, M.; Saykina, V.; de Bivort, B. Neural mechanisms of parasite-induced summiting behavior in 'zombie' *Drosophila*. *eLife* **2023**, *12*, e85410. [CrossRef]
36. Moro, C.A.; Sony, S.A.; Franklin, L.P.; Dong, S.; Peifer, M.M.; Wittig, K.E.; Hanna-Rose, W. Adenylosuccinate lyase deficiency affects neurobehavior via perturbations to tyramine signaling in *Caenorhabditis elegans*. *PLoS Genet.* **2023**, *19*, e1010974. [CrossRef]
37. Feng, M.; Fei, S.; Xia, J.; Zhang, M.; Wu, H.; Swevers, L.; Sun, J. Global Metabolic Profiling of Baculovirus Infection in Silkworm Hemolymph Shows the Importance of Amino-Acid Metabolism. *Viruses* **2021**, *13*, 841. [CrossRef]
38. Qian, H.; Guo, H.; Zhang, X.; Liu, M.; Zhao, G.; Xu, A.; Li, G. Metabolic characterization of hemolymph in *Bombyx mori* varieties after *Bombyx mori* nucleopolyhedrovirus infection by GC-MS-based metabolite profiling. *Arch. Virol.* **2022**, *167*, 1637–1648. [CrossRef]

39. Shi, X.; Zhang, Y.; Zhu, T.; Li, N.; Sun, S.; Zhu, M.; Pan, J.; Shen, Z.; Hu, X.; Zhang, X.; et al. Response to *Bombyx mori* nucleopolyhedrovirus infection in silkworm: Gut metabolites and microbiota. *Dev. Comp. Immunol.* **2021**, *125*, 104227. [CrossRef]
40. Qian, H.; Li, G.; Zhao, G.; Liu, M.; Xu, A. Metabolic Characterisation of the Midgut of *Bombyx mori* Varieties after BmNPV Infection Using GC-MS-Based Metabolite Profiling. *Int. J. Mol. Sci.* **2020**, *21*, 4707. [CrossRef]
41. Zhao, P.; Rensing, C.; Wang, D. Symbiotic Bacteria Modulate *Lymantria dispar* Immunity by Altering Community Proportions after Infection with LdMNPV. *Int. J. Mol. Sci.* **2023**, *24*, 9694. [CrossRef]
42. Kim, D.; Paggi, J.M.; Park, C.; Bennett, C.; Salzberg, S.L. Graph-based genome alignment and genotyping with HISAT2 and HISAT-genotype. *Nat. Biotechnol.* **2019**, *37*, 907–915. [CrossRef]
43. Kovaka, S.; Zimin, A.V.; Pertea, G.M.; Razaghi, R.; Salzberg, S.L.; Pertea, M. Transcriptome assembly from long-read RNA-seq alignments with StringTie2. *Genome Biol.* **2019**, *20*, 278. [CrossRef]
44. Love, M.I.; Huber, W.; Anders, S. Moderated estimation of fold change and dispersion for RNA-seq data with DESeq2. *Genome Biol.* **2014**, *15*, 550. [CrossRef]
45. Wu, T.; Hu, E.; Xu, S.; Chen, M.; Guo, P.; Dai, Z.; Feng, T.; Zhou, L.; Tang, W.; Zhan, L.; et al. clusterProfiler 4.0: A universal enrichment tool for interpreting omics data. *Innovation* **2021**, *2*, 100141. [CrossRef]
46. Subramanian, A.; Tamayo, P.; Mootha, V.K.; Mukherjee, S.; Ebert, B.L.; Gillette, M.A.; Paulovich, A.; Pomeroy, S.L.; Golub, T.R.; Lander, E.S.; et al. Gene set enrichment analysis: A knowledge-based approach for interpreting genome-wide expression profiles. *Proc. Natl. Acad. Sci. USA* **2005**, *102*, 15545–15550. [CrossRef]
47. Desai, R.I.; Kangas, B.D.; Luc, O.T.; Solakidou, E.; Smith, E.C.; Dawes, M.H.; Ma, X.; Makriyannis, A.; Chatterjee, S.; Dayeh, M.A.; et al. Complex 33-beam simulated galactic cosmic radiation exposure impacts cognitive function and prefrontal cortex neurotransmitter networks in male mice. *Nat. Commun.* **2023**, *14*, 7779. [CrossRef]
48. Adams, K.J.; Pratt, B.; Bose, N.; DuBois, L.G.; St. John-Williams, L.; Perrott, K.M.; Ky, K.; Kapahi, P.; Sharma, V.; MacCoss, M.J.; et al. Skyline for Small Molecules: A Unifying Software Package for Quantitative Metabolomics. *J. Proteome Res.* **2020**, *19*, 1447–1458. [CrossRef]
49. Wang, Q.; Yin, M.; Yuan, C.; Liu, X.; Hu, Z.; Zou, Z.; Wang, M. Identification of a Conserved Prophenoloxidase Activation Pathway in Cotton Bollworm *Helicoverpa armigera*. *Front. Immunol.* **2020**, *11*, 785. [CrossRef]
50. Toufeeq, S.; Wang, J.; Zhang, S.Z.; Li, B.; Hu, P.; Zhu, L.B.; You, L.L.; Xu, J.P. Bmserpin2 Is Involved in BmNPV Infection by Suppressing Melanization in *Bombyx mori*. *Insects* **2019**, *10*, 399. [CrossRef]
51. Liu, L.; Wang, D. Four antimicrobial peptides of Asian gypsy moth respond to infection of its viral pathogen, nucleopolyhedrovirus (LdMNPV). *Pestic. Biochem. Physiol.* **2023**, *190*, 105335. [CrossRef]
52. Liu, L.; Wei, Y.S.; Wang, D. Identification of Core Genes of Toll-like Receptor Pathway from *Lymantria dispar* and Induced Expression upon Immune Stimulant. *Insects* **2021**, *12*, 827. [CrossRef]
53. O'Donnell, M.P.; Fox, B.W.; Chao, P.H.; Schroeder, F.C.; Sengupta, P. A neurotransmitter produced by gut bacteria modulates host sensory behaviour. *Nature* **2020**, *583*, 415–420. [CrossRef]
54. Yuan, C.; Xing, L.; Wang, M.; Hu, Z.; Zou, Z. Microbiota modulates gut immunity and promotes baculovirus infection in *Helicoverpa armigera*. *Insect Sci.* **2021**, *28*, 1766–1779. [CrossRef]

Disclaimer/Publisher's Note: The statements, opinions and data contained in all publications are solely those of the individual author(s) and contributor(s) and not of MDPI and/or the editor(s). MDPI and/or the editor(s) disclaim responsibility for any injury to people or property resulting from any ideas, methods, instructions or products referred to in the content.